Accurate quantum chemical reaction energies for lithium-mediated electrolyte decomposition and evaluation of density functional approximations

Sibali Debnath,[†] Verena A. Neufeld,[†,‡] Leif D. Jacobson,[¶] Benjamin Rudshteyn,[§] John L. Weber,[†] Timothy C. Berkelbach,[*,†] and Richard A. Friesner[*,†,§]

[†]*Department of Chemistry, Columbia University, New York, NY, 10027, United States*

[‡]*Division of Chemistry and Chemical Engineering, California Institute of Technology, Pasadena, CA, 91125, United States*

[¶]*Schrödinger, Inc., Portland, OR 97204, United States*

[§]*Schrödinger, Inc., New York, NY 10036, United States*

E-mail: t.berkelbach@columbia.edu; raf8@columbia.edu

Abstract

An important concern related to the performance of Li ion batteries is the formation of the solid electrolyte interphase on the surface of the anode. This film is formed from the decomposition of electrolytes and can have important effects on stability and performance. Here, we evaluate the decomposition pathway of ethylene carbonate and related organic electrolyte molecules using a series of density functional approximations and correlated wavefunction (WF) methods, including coupled-cluster theory with single, double, and perturbative triple excitations [CCSD(T)] and auxiliary field quantum Monte Carlo (AFQMC). We find that the transition state barrier associated with ring opening varies widely across different functionals, ranging from 3.00 to 17.15 kcal/mol, which can be compared to the value of 12.84 kcal/mol predicted by CCSD(T).This large variation underscores the importance of benchmarking against accurate WF methods. A performance comparison of all the density functionals used in this study reveals that dispersion-corrected M06-2X (a meta-hybrid GGA), CAM-B3LYP (a range-separated hybrid) and B2GP-PLYP (a double-hybrid) perform the best, with average errors of about 1.60 kcal/mol compared to CCSD(T). We also compared the performance of WF methods that are more scalable than CCSD(T), finding that DLPNO-CCSD(T) and phaseless AFQMC with a DFT trial wavefunction exhibit average errors of 1.38 kcal/mol and 1.74 kcal/mol respectively.

1 Introduction

Lithium-ion batteries have been the gold standard and ubiquitous driving force behind almost all electronic devices for over two decades.[1,2] A typical lithium-ion battery consist of a graphite anode, a transition metal oxide cathode, and an electrically insulating and ionically conducting nonaqueous organic electrolyte that acts as an ionic path between the two.[3,4] One key to understanding a battery's electrochemistry is its electrode/electrolyte interface, which controls critical aspects of performance and is thus a target for improvement.[5,6] The decomposition of organic electrolyte molecules at the electrode surface yields a passivation

layer called the solid electrolyte interphase (SEI).[7] Understanding the SEI layer formation, composition, and growth over multiple time and length scales is essential for the design of next-generation safe and performant lithium-ion batteries.[8,9]

The most common electrolytes are mixtures of alkyl carbonates such as ethylene carbonate (EC) or propylene carbonate (PC), and lithium salts such as $LiAsF_6$ or $LiPF_6$.[10] Both components undergo chemical reactions that contribute to the composition of the SEI. The choice of an electrolyte is partially based on its compatibility with the electrode materials used, such that the electrolyte should either be electrochemically stable or form a stable and well-understood SEI at the electrode surface,[6] necessitating a thorough understanding of the electrolyte stability and decomposition pathways. However, it is experimentally challenging to directly capture reactive processes leading to the formation of SEI.[11,12]

Alternatively, atomistic simulations, including electronic structure theory and molecular dynamics, have the potential to contribute to a fundamental understanding of the electrolyte decomposition pathways responsible for the SEI.[13–19] Although density functional theory (DFT) has become a standard approach due to the steep computational scaling of more accurate wavefunction (WF) methods that explicitly describe electron correlation, the results can vary depending on the density functional approximation used and the system of interest. Therefore, the selection of a particular density functional approximation for a specific application requires rigorous benchmarking studies.[20–24] In this work, we carry out such a study for the problem of organic electrolyte decomposition in the presence of lithium.

Specifically, we study the reductive decomposition of the organic electrolytes ethylene carbonate (EC), propylene carbonate (PC), and fluoroethylene carbonate (FEC). The reaction pathways studied here are similar to those investigated previously by Balbuena and coworkers[25] using DFT. We perform accurate benchmark calculations using a variety of high level WF methods, and then evaluate a range of DFT functionals; our work should be useful for the future development of accurate force field parameters for large scale atomistic simulations of battery electrochemistry.[26,27] In addition to our evaluation of a range of DFT function-

als, we also use the EC decomposition to compare three accurate WF methods capable of serving as a benchmark: coupled-cluster theory with single, double, and perturbative triple excitations [CCSD(T)],[28] its low-scaling variant via domain-based local pair natural orbitals [DLPNO-CCSD(T)],[29] and phaseless auxiliary field quantum Monte Carlo (ph-AFQMC) using a Kohn-Sham determinant trial wavefunction. We find that the three methods yield similar reactions energetics (within a few kcal/mol), and this internal consistency—especially between very different methods like coupled cluster and AFQMC—supports the conclusion that all three give accurate results for this class of reactions. Consequently, we utilize the least expensive approach, DLPNO-CCSD(T), in studying the remaining reactions (involving the PC and FEC electrolyte solvent components). It should be noted, however, that if the desired precision was chemical accuracy (1 kcal/mol), further improvement of the reference results would be necessary.

2 Methods

All geometry optimizations are performed at the ωB97X-D/def2-TZVP(-f) level of theory using Jaguar v11.4.[30] The transition state (TS) of the EC decomposition pathway is obtained using the automatic transition state (AutoTS) search approach as detailed in Ref. 31. The transition states of the substituted ethylene carbonates (FEC and PC) are initially optimized with the eigenvector following method using ωB97X-D/6-31G* as a guess, followed by frequency analysis to verify the TS. Finally, these pre-optimized TS geometries were refined with eigenvector following utilizing ωB97X-D/def2-TZVP(-f). These geometries are used for all subsequent energy evaluations.

DFT single-point energy calculations were performed with Jaguar v11.4 and Orca v5.0 using the def2-TZVP(-f) basis set, without any further basis set extrapolation. We selected a wide range of DFT functionals belonging to different rungs of Jacob's ladder, including generalized gradient approximation (GGA), meta-GGA, hybrid, meta-hybrid-GGA, range-

separated hybrid, and double hybrid.[32] Many of the functionals were combined with various treatments of dispersion, including D3,[33] D3BJ,[34] and VV10.[35] The full list of density functional approximations can be found in Sec. 3. In total, we tested 17 different density functional approximations.

Canonical CCSD and CCSD(T) calculations were performed with PySCF v1.7.[36–38]

DLPNO-CCSD and DLPNO-CCSD(T) calculations were performed with ORCA 5.0[39] using "TightPNO" settings and semi-canonical perturbative triple corrections (i.e., without the improved iterative "(T1)" correction[40]).All CC calculations were performed using a spin-unrestricted Hartree-Fock (HF) reference determinant and core orbitals were frozen. All AFQMC calculations were carried out using single determinant trial wavefunctions as detailed in Ref. 41. The trial wavefunctions (UB3LYP) and integrals for AFQMC were obtained with PySCF v2.0. Similar to previous studies,[42] the imaginary time step for the AFQMC propagation was 0.005 Ha^{-1}, and the total propagation time was 200 Ha^{-1}, employing the "comb" algorithm for population control every 20 steps.[43] We used 3312 total walkers, which were initialized with a spin-restricted HF determinant.

Calculations were performed with the aug-cc-pVDZ, TZ, and QZ basis sets. The HF energy was extrapolated to the CBS limit with an exponential form and the correlation energy was extrapolated with a $X^{-3.05}$ form,[44] using the TZ and QZ results ($X = 2, 3, 4$ for DZ, TZ, QZ). As one exception, the reaction involving formation of **8** was too large to treat at the QZ level with CC theory, so extrapolation was performed with a $X^{-2.51}$ form using only DZ and TZ results.[44]

In this work, we focus on the purely electronic energies, i.e., we neglect vibrational corrections and all calculations are performed in the gas phase. This approach facilitates a direct comparison of different levels of electronic structure theory, but of course is not meant to be compared to experimental values. Although we expect small vibrational corrections on the order of 1–2 kcal/mol, the solvation energy corrections are expected to be very large. Nonetheless, we expect our conclusions concerning the performance of different levels of

theory to hold even when the solvent is treated explicitly or implicitly.

3 Results and Discussion

We study in detail the reductive decomposition of ethylene carbonate (EC) in the presence of a lithium ion, and we closely follow the mechanism identified in Ref. 25. We also study the same reaction for propylene carbonate (PC) and fluoroethylene carbonate (FEC), as a confirmation of the generality of our conclusions.

3.1 Reductive decomposition of ethylene carbonate

Figure 1 illustrates the steps of the reductive decomposition of EC.[25] Step 1 involves the strong binding of the EC molecule **1** with a Li^+ ion to form the ion-pair intermediate **2**.This ion-pair intermediate **2** is reduced in step 2 to form the neutral adduct **3**; the energy change for this step is large and negative due to the strong electron affinity induced by the Li^+ ion (in the absence of Li^+, addition of an electron to gas phase EC requires about +8 kcal/mol).[25] The adduct **3** subsequently undergoes homolytic ring cleavage, passing through the transition state **4** in step 3 to form the intermediate radical **5** in step 4. A nonplanar pathway in steps 2 and 3 is also possible,[25] but we do not consider it here. Once the radical **5** is formed, there are several possible termination pathways. Here, we study two such pathways, as illustrated in step 5 and 6, which correspond to pathways **C** and **B**, respectively, in Ref. 25. The first is a reductive decomposition to form lithium carbonate anion **6** and ethylene **7**. The second is a dimerization of the radical **5** to form ethylene **7** and lithium ethylene dicarbonate **8**. We note that both lithium carbonate and lithium ethylene dicarbonate have been implicated as major components of the SEI, but there are some conflicting observations.[45–47]

Using the electronic structure methods described in Sec. 2, we calculated the electronic energy differences of all six steps. A T1 diagnostic test[48] on CC calculations confirms that all species are qualitatively single-reference, supporting the application of DFT, CC, and

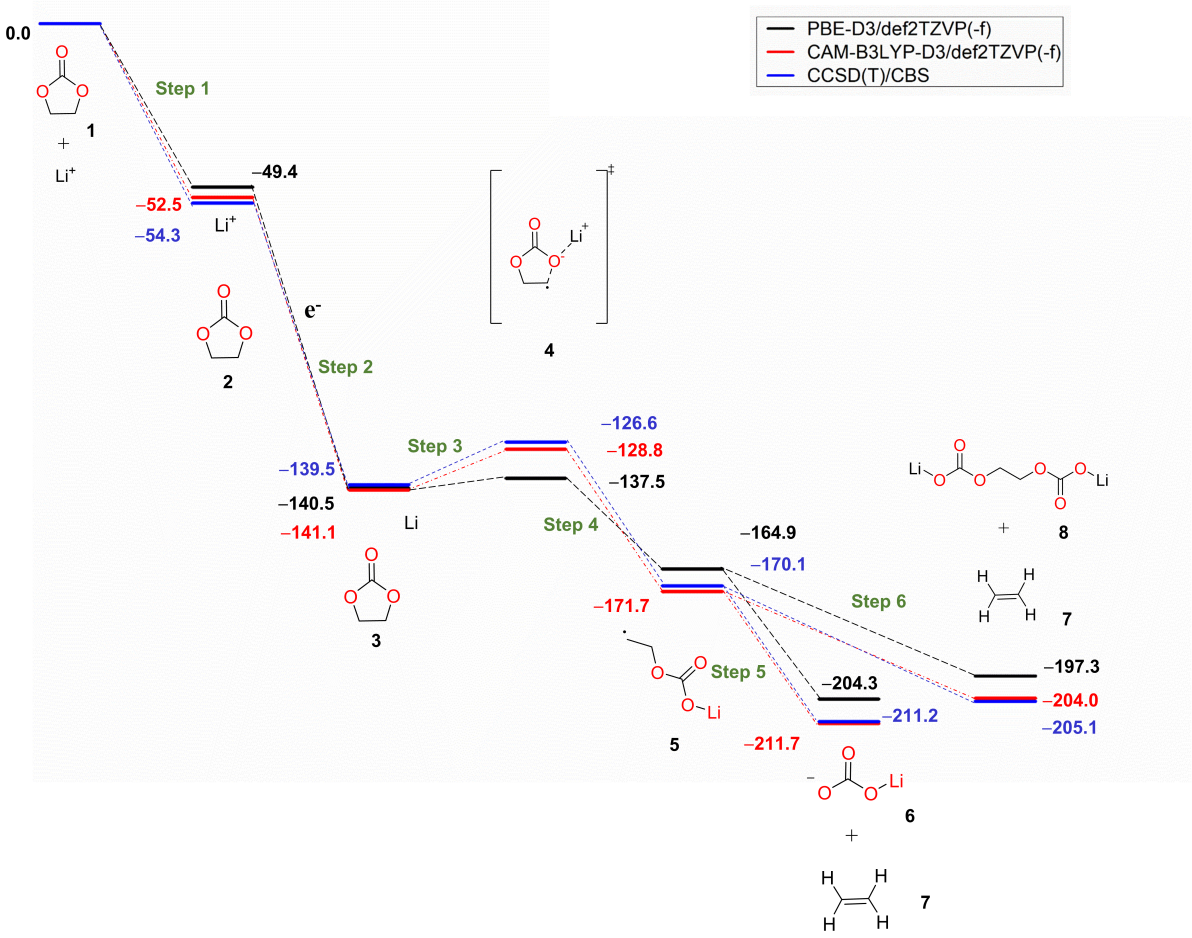

Figure 1: Reductive decomposition of EC in the presence of a lithium ion calculated using three different levels of theory. Relative energies with respect to the initial species are given in kcal/mol.

AFQMC with a single determinant trial. Using CCSD(T) as the reference, we then calculate the mean absolute deviation (MAD) over these six steps for each method considered. The detailed reaction energy profile predicted by PBE-D3, CAM-B3LYP-D3, and CCSD(T) is shown in Figure 1 and the MAD from all methods is presented in Figure 2.

First, we consider the performance of the wavefunction methods. Among those we tested, DLPNO-CCSD(T) has the the smallest MAD of 1.38 kcal/mol, where the largest deviations of 2.70 kcal/mol and 3.01 kcal/mol are observed for the reactions involving the transition state (steps 3 and 4), which is consistent with other reports of overestimations of transition state barriers by DLPNO-CCSD(T).[49] Without step 3 and step 4, the MAD of

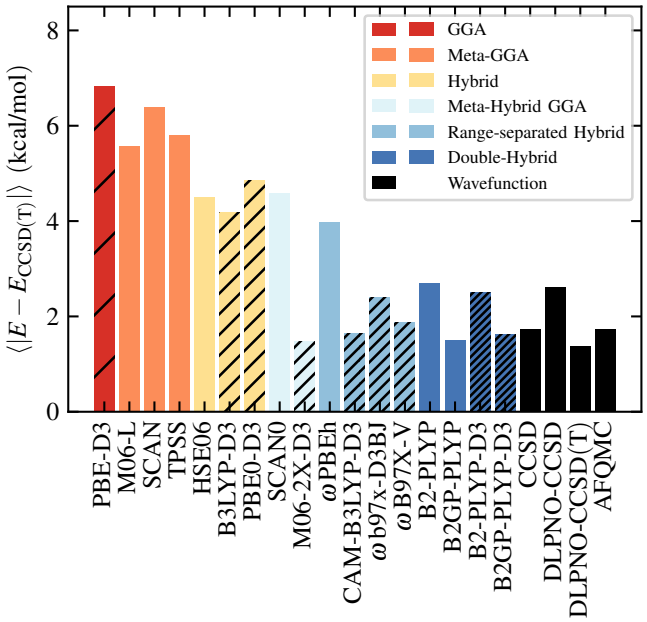

Figure 2: Mean absolute deviation with respect to CCSD(T) of stepwise energy differences for the reductive decomposition of EC shown in Fig. 1.

DLPNO-CCSD(T) is reduced to 0.64 kcal/mol, which is excellent in light of its significantly lower computational cost compared to canonical CCSD(T).The MADs obtained for CCSD, DLPNO-CCSD, and AFQMC are 1.73 kcal/mol, 2.61 kcal/mol, and 1.74 kcal/mol, respectively, where AFQMC has an average statistical uncertainty of ±1.10 kcal/mol. Again, the highest deviations are obtained for steps 3 and 4. As shown in Figures 3 and 4, all other wavefunction methods overestimate barrier heights compared to CCSD(T), which is opposite to the behavior displayed by most density functionals. Overall, the wavefunction methods are reasonably consistent, justifying their usage as a benchmark, and the good performance of DLPNO-CCSD(T) supports its application to larger molecular systems than accessible with canonical CCSD(T).

Turning to the performance of DFT, we see that PBE-D3, arguably the most popular GGA functional in battery modelling, has a large MAD of 6.83 kcal/mol. The meta-GGAs M06-L, SCAN and TPSS exhibit MADs between 5.50 and 6.40 kcal/mol. These results raise concerns about the reliability of commonly used functionals for applications related to SEI

modelling. Hybrids perform slightly better, with MADs between 4.00 and 5.00 kcal/mol, with the lowest MAD of 4.18 kcal/mol for B3LYP-D3. The meta-hybrid functional M06-2X-D3 performs best, with an MAD of 1.48 kcal/mol, which is comparable to DLPNO-CCSD(T). However, the other meta-hybrid SCAN0 exhibits a relatively large MAD of 4.59 kcal/mol, with the largest deviation of 11.26 kcal/mol obtained for step 5 (reductive decomposition). The range-separated hybrid functionals also perform well, especially when dispersion corrections are included. The lowest MAD is obtained for CAM-B3LYP-D3 (1.64 kcal/mol). The MAD of other leading range-separated hybrid functionals, such as ωB97X-D3BJ and ωB97X-V is about 1.80–2.40 kcal/mol. The double-hybrid functionals give similar average errors ranging from 1.50–2.70 kcal/mol, with B2GP-PLYP(-D3) having the lowest MAD of less than 2.00 kcal/mol. Based on all of these results we can identify dispersion-corrected M06-2X (meta-hybrid GGA), CAM-B3LYP and ωB97X (range-separated hybrids), and B2GPLYP (double hybrid) as among the best performing functionals.

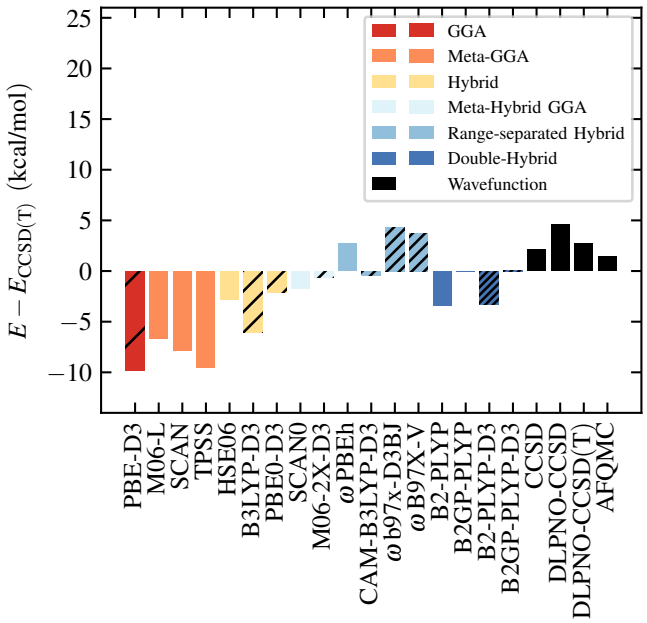

Figure 3: Signed deviation with respect to CCSD(T) for the transition state barrier for ring opening (step 3).

In the SI (SI-1.1), we provide errors for each step of the decomposition pathway from

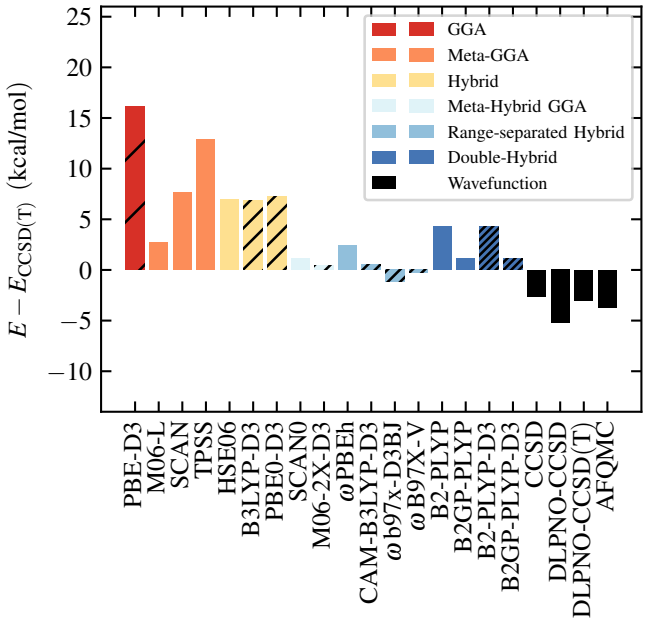

Figure 4: Signed deviation with respect to CCSD(T) for step 4, which is the reverse of a transition state for the ring closing reaction.

all methods, which provides a more detailed look into their performance. Here, we focus on their performance for the critical step 3, i.e., the transition state barrier for ring opening, which determines the kinetics of the decomposition.Figure 3 shows the absolute deviation of all methods with respect to CCSD(T) for this step. The deviation ranges from 0.02–9.84 kcal/mol, with B2GPLYP-D3 (0.02 kcal/mol), B2GPLYP (0.04 kcal/mol), CAM-B3LYP-D3 (0.44 kcal/mol), and M062X-D3 (0.64 kcal/mol) agreeing well with the reference value. While ωB97X-V has a mean error of 1.88 kcal/mol when averaged over all reaction steps, it exhibits a significant error of 3.74 kcal/mol for this critical step. Importantly, we find that some of the most common functionals used for materials simulations resulted in large deviations. For example, PBE-D3, SCAN, TPSS, and B3LYP-D3 underestimate the barrier height by more than 6 kcal/mol. Similar behavior is seen for step 4, which is to be expected because the magnitude of its energy difference is the barrier height for the reversed (ring closing) reaction. As shown in Figure 4, the error for this step closely tracks that of the ring-opening barrier height (step 3), but with opposite sign. The observed challenge in

describing the energy differences of these steps is presumably due to the self-interaction error and associated stabilization of delocalized electronic structure of the transition state geometry **4**. Although we observe an improvement by over 7 kcal/mol for PBE0-D3 compared to PBE-D3 for these steps, attributable to its reduced self-interaction error, such improvement is not consistent across all steps of the reaction. For example, in steps 5 and 6 (Figure S3a and Figure S3b), the errors obtained for PBE0-D3 are larger than for PBE-D3. Thus, it is difficult to rank PBE0-D3 and PBE-D3 for this reaction pathway.

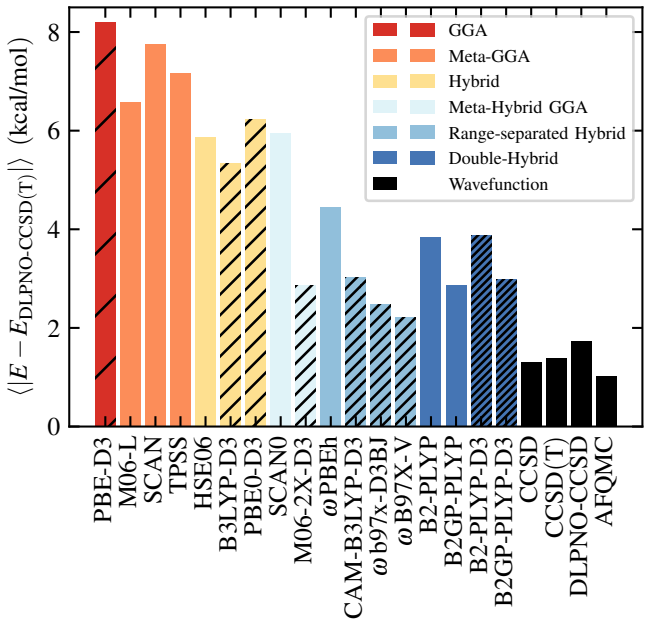

Figure 5: MAD of DFT functionals and wave function methods with respect to DLPNO-CCSD(T).

This completes our analysis of the reductive decomposition of EC, but before moving on, we note that exhaustive benchmarking against CCSD(T) is computationally expensive, especially for increasingly large molecules. DLPNO-CCSD(T) provides a cheaper alternative to serve as a benchmark, especially given its good agreement with canonical CCSD(T).To test whether our conclusions are changed, we repeated the same analysis using DLPNO-CCSD(T) as the reference, and the results are shown in Figure 5. Overall, we observe very similar trends, although the MAD of almost all functionals is increased by about 0.50–

1.40 kcal/mol due to errors introduced by the DLPNO approximations. For example, the 2.69 kcal/mol overestimation of the barrier height (step 3) by DLPNO-CCSD(T) changes the apparent accuracy of one of the best performing functionals, M06-2X-D3, from 0.63 kcal/mol to 3.33 kcal/mol. This effect needs to be kept in mind when benchmarking DFT functionals against affordable DLPNO-CCSD(T) calculations.

To test the transferability of our conclusions above with regard to functional performance, we extended our study to two electrolyte solvent molecules with substitution, $-CH_3$ and $-F$ (PC and FEC). Given the comparatively cheaper cost and good performance of DLPNO-CCSD(T) with respect to CCSD(T), we select DLPNO-CCSD(T) as the reference to compare the performance of different density functionals. Our detailed numerical results are given in the SI (SI-2 and SI-3), but, unsurprisingly, the findings are very similar to those for EC, reinforcing our previous conclusions. Specifically, B3LYP-D3, M06-2X-D3, CAM-B3LYP-D3, and the double-hybrids are the best performing functionals within their respective rungs.

4 Conclusion

In this work, we have benchmarked different density functionals against accurate correlated WF methods for lithium-mediated electrolyte decomposition. In addition, we have compared the agreement between different correlated methods. Overall, DLPNO-CCSD(T) shows good agreement with canonical CCSD(T) for the reaction energies: when the reactions involving transition state is excluded, the MAD is 0.64 kcal/mol. Moreover, AFQMC also shows good agreement with a MAD of 1.74 kcal/mol and an average statistical uncertainty of ± 1 kcal/mol. Considering the accuracy and cost of different correlated methods, we conclude that DLPNO-CCSD(T) is an excellent benchmark method for reaction energies of complex systems relevant to battery electrochemistry, i.e., reactions involving organic molecules and Li atoms. For barrier heights, it would likely help to improve the quality of the DLPNO-CCSD(T) calculations via tightened parameters (TCutPNO, TCutMKN, TCutPairs)[49] and

usage of the improved iterative "(T1)" correction.[40]

A performance comparison of all the density functional approximations used in this study reveals that CAM-B3LYP-D3, M06-2X-D3, and double-hybrids perform very well for this system. Perhaps most importantly, the DFT transition state barrier heights vary from 3.00 to 17.15 kcal/mol, when the CCSD(T) barrier height is 12.84 kcal/mol. GGAs in particular are especially prone to significant underestimation of the barrier height by up to 10 kcal/mol. Therefore, we urge caution when interpreting the results of GGA-based molecular dynamics simulations of electrolyte decomposition and SEI formation.However, despite the good performance of meta-GGAs, range-separated hybrids, and double-hybrids observed in this molecular study, we note that these families of functionals are limited in their applicability to periodic metals.[50] The development of accurate and broadly applicable electronic structure methods for surface chemistry is an important task for the community, especially towards the development of accurate force fields for reactive molecular dynamics simulations.

5 Acknowledgment

This work was supported by the Columbia Center for Computational Electrochemistry. We acknowledge computing resources from Columbia University's Shared Research Computing Facility project, which is supported by NIH Research Facility Improvement Grant 1G20RR030893-01, and associated funds from the New York State Empire State Development, Division of Science Technology and Innovation (NYSTAR) Contract C090171, both awarded April 15, 2010. This research used resources of the Oak Ridge Leadership Computing Facility at the Oak Ridge National Laboratory, which is supported by the Office of Science of the U.S. Department of Energy under Contract DE-AC05-00OR22725. B.R. acknowledges funding from the National Institute of General Medical Sciences of the National Institutes of Health under award number F32GM136105.

6 Associated Content

The supporting information includes

- Individual reaction energies of ethylene carbonate decomposition pathway
- Individual reaction energies of fluoroethylene carbonate decomposition pathway
- Individual reaction energies of propylene carbonate decomposition pathway

7 Author Information

Corresponding Authors

Richard A. Friesner — Department of Chemistry, Columbia University, New York, NY, 10027, United States, Schrödinger, Inc., New York, NY 10036, United States; Email: raf8@columbia.edu

Timothy C. Berkelbach — Department of Chemistry, Columbia University, New York, NY, 10027; Email: t.berkelbatch@columbia.edu

Authors

Sibali Debnath — Department of Chemistry, Columbia University, New York, NY, 10027

Verena A. Neufeld — Department of Chemistry, Columbia University, New York, NY, 10027, Division of Chemistry and Chemical Engineering, California Institute of Technology, Pasadena, CA, 91125, United States

Leif D. Jacobson — Schrödinger, Inc., Portland, OR 97204, United States

Benjamin Rudshteyn — Schrödinger, Inc., New York, NY 10036, United States

John L. Weber — Department of Chemistry, Columbia University, New York, NY, 10027, United States

Notes

The authors declare the following competing financial interest(s): R.A.F. has a significant financial stake in, is a consultant for, and is on the Scientific Advisory Board of Schrödinger, Inc.

References

(1) Hou, J.; Lu, L.; Wang, L.; Ohma, A.; Ren, D.; Feng, X.; Li, Y.; Li, Y.; Ootani, I.; Han, X. et al. Thermal runaway of Lithium-ion batteries employing LiN (SO2F) 2-based concentrated electrolytes. *Nat. Commun.* **2020**, *11*, 1–11.

(2) Wang, A.; Kadam, S.; Li, H.; Shi, S.; Qi, Y. Review on modeling of the anode solid electrolyte interphase (SEI) for lithium-ion batteries. *Npj Comput. Mater.* **2018**, *4*, 1–26.

(3) Nitta, N.; Wu, F.; Lee, J. T.; Yushin, G. Li-ion battery materials: present and future. *Mater Today* **2015**, *18*, 252–264.

(4) Bhatt, M. D.; O'Dwyer, C. Density functional theory calculations for ethylene carbonate-based binary electrolyte mixtures in lithium ion batteries. *Curr. Appl. Phys.* **2014**, *14*, 349–354.

(5) Peled, E.; Menkin, S. SEI: past, present and future. *J. Electrochem. Soc.* **2017**, *164*, A1703.

(6) An, S. J.; Li, J.; Daniel, C.; Mohanty, D.; Nagpure, S.; Wood III, D. L. The state of understanding of the lithium-ion-battery graphite solid electrolyte interphase (SEI) and its relationship to formation cycling. *Carbon* **2016**, *105*, 52–76.

(7) Peled, E. The electrochemical behavior of alkali and alkaline earth metals in nonaqueous battery systems—the solid electrolyte interphase model. *J. Electrochem. Soc.* **1979**, *126*, 2047.

(8) Lu, H.; Zhu, Y.; Zheng, B.; Du, H.; Zheng, X.; Liu, C.; Yuan, Y.; Fang, J.; Zhang, K. A hybrid ionic liquid-based electrolyte for high-performance lithium–sulfur batteries. *New J. Chem.* **2020**, *44*, 361–368.

(9) Yu, Z.; Wang, H.; Kong, X.; Huang, W.; Tsao, Y.; Mackanic, D. G.; Wang, K.; Wang, X.; Huang, W.; Choudhury, S. et al. Molecular design for electrolyte solvents enabling energy-dense and long-cycling lithium metal batteries. *Nat. Energy* **2020**, *5*, 526–533.

(10) Wang, Y.; Balbuena, P. B. Theoretical insights into the reductive decompositions of propylene carbonate and vinylene carbonate: density functional theory studies. *J. Phys. Chem. B* **2002**, *106*, 4486–4495.

(11) Adenusi, H.; Chass, G. A.; Passerini, S.; Tian, K. V.; Chen, G. Lithium Batteries and the Solid Electrolyte Interphase (SEI)—Progress and Outlook. *Adv. Energy Mater.* **2023**, *13*, 2203307.

(12) Edström, K.; Herstedt, M.; Abraham, D. P. A new look at the solid electrolyte interphase on graphite anodes in Li-ion batteries. *J. Power Sources* **2006**, *153*, 380–384.

(13) Leung, K.; Budzien, J. L. Ab initio molecular dynamics simulations of the initial stages of solid–electrolyte interphase formation on lithium ion battery graphitic anodes. *Phys. Chem. Chem. Phys.* **2010**, *12*, 6583–6586.

(14) Leung, K.; Rempe, S. B.; Foster, M. E.; Ma, Y.; del la Hoz, J. M. M.; Sai, N.; Balbuena, P. B. Modeling electrochemical decomposition of fluoroethylene carbonate on silicon anode surfaces in lithium ion batteries. *J. Electrochem. Soc.* **2013**, *161*, A213.

(15) Silva, L. B.; Freitas, L. C. G. Structural and thermodynamic properties of liquid ethylene carbonate and propylene carbonate by Monte Carlo Simulations. *J. Mol. Struct.* **2007**, *806*, 23–34.

(16) Borodin, O.; Smith, G. D. Quantum chemistry and molecular dynamics simulation study of dimethyl carbonate: ethylene carbonate electrolytes doped with LiPF6. *J. Phys. Chem. B* **2009**, *113*, 1763–1776.

(17) Islam, M. M.; Van Duin, A. C. Reductive decomposition reactions of ethylene carbonate by explicit electron transfer from lithium: an eReaxFF molecular dynamics study. *J. Phys. Chem. C* **2016**, *120*, 27128–27134.

(18) Kim, S.-P.; Van Duin, A. C.; Shenoy, V. B. Effect of electrolytes on the structure and evolution of the solid electrolyte interphase (SEI) in Li-ion batteries: A molecular dynamics study. *J. Power Sources* **2011**, *196*, 8590–8597.

(19) Yu, J.; Balbuena, P. B.; Budzien, J.; Leung, K. Hybrid DFT functional-based static and molecular dynamics studies of excess electron in liquid ethylene carbonate. *J. Electrochem. Soc.* **2011**, *158*, A400.

(20) Mardirossian, N.; Head-Gordon, M. Thirty years of density functional theory in computational chemistry: an overview and extensive assessment of 200 density functionals. *Mol. Phys.* **2017**, *115*, 2315–2372.

(21) Risthaus, T.; Grimme, S. Benchmarking of London dispersion-accounting density functional theory methods on very large molecular complexes. *J. Chem. Theory Comput.* **2013**, *9*, 1580–1591.

(22) Krieg, H.; Grimme, S. Thermochemical benchmarking of hydrocarbon bond separation reaction energies: Jacob's ladder is not reversed! *Mol. Phys.* **2010**, *108*, 2655–2666.

(23) Gruden, M.; Andjeklović, L.; Jissy, A. K.; Stepanović, S.; Zlatar, M.; Cui, Q.; Elstner, M. Benchmarking density functional tight binding models for barrier heights and reaction energetics of organic molecules. *J. Comput. Chem.* **2017**, *38*, 2171–2185.

(24) Maurer, L. R.; Bursch, M.; Grimme, S.; Hansen, A. Assessing density functional theory for chemically relevant open-shell transition metal reactions. *J. Chem. Theory Comput.* **2021**, *17*, 6134–6151.

(25) Wang, Y.; Nakamura, S.; Ue, M.; Balbuena, P. B. Theoretical studies to understand surface chemistry on carbon anodes for lithium-ion batteries: reduction mechanisms of ethylene carbonate. *J. Am. Chem. Soc.* **2001**, *123*, 11708–11718.

(26) Yun, K.-S.; Pai, S. J.; Yeo, B. C.; Lee, K.-R.; Kim, S.-J.; Han, S. S. Simulation protocol for prediction of a solid-electrolyte interphase on the silicon-based anodes of a lithium-ion battery: ReaxFF reactive force field. *J. Phys. Chem. Lett.* **2017**, *8*, 2812–2818.

(27) Dajnowicz, S.; Agarwal, G.; Stevenson, J. M.; Jacobson, L. D.; Ramezanghorbani, F.; Leswing, K.; Friesner, R. A.; Halls, M. D.; Abel, R. High-dimensional neural network potential for liquid electrolyte simulations. *J. Phys. Chem. B* **2022**, *126*, 6271–6280.

(28) Raghavachari, K.; Trucks, G. W.; Pople, J. A.; Head-Gordon, M. A fifth-order perturbation comparison of electron correlation theories. *Chem. Phys. Lett.* **1989**, *157*, 479–483.

(29) Riplinger, C.; Sandhoefer, B.; Hansen, A.; Neese, F. Natural triple excitations in local coupled cluster calculations with pair natural orbitals. *J. Chem. Phys.* **2013**, *139*, 134101.

(30) Bochevarov, A. D.; Harder, E.; Hughes, T. F.; Greenwood, J. R.; Braden, D. A.; Philipp, D. M.; Rinaldo, D.; Halls, M. D.; Zhang, J.; Friesner, R. A. Jaguar: A high-performance quantum chemistry software program with strengths in life and materials sciences. *Int. J. Quantum Chem.* **2013**, *113*, 2110–2142.

(31) Jacobson, L. D.; Bochevarov, A. D.; Watson, M. A.; Hughes, T. F.; Rinaldo, D.; Ehrlich, S.; Steinbrecher, T. B.; Vaitheeswaran, S.; Philipp, D. M.; Halls, M. D. et al.

Automated transition state search and its application to diverse types of organic reactions. *J. Chem. Theory Comput.* **2017**, *13*, 5780–5797.

(32) Perdew, J. P.; Schmidt, K. Jacob's ladder of density functional approximations for the exchange-correlation energy. AIP Conf. Proc. 2001; pp 1–20.

(33) Grimme, S. Density functional theory with London dispersion corrections. *Wiley Interdiscip. Rev. Comput. Mol. Sci.* **2011**, *1*, 211–228.

(34) Grimme, S.; Ehrlich, S.; Goerigk, L. Effect of the damping function in dispersion corrected density functional theory. *J. Comput. Chem.* **2011**, *32*, 1456–1465.

(35) Vydrov, O. A.; Wu, Q.; Van Voorhis, T. Self-consistent implementation of a nonlocal van der Waals density functional with a Gaussian basis set. *J. Chem. Phys.* **2008**, *129*, 014106.

(36) Sun, Q.; Berkelbach, T. C.; Blunt, N. S.; Booth, G. H.; Guo, S.; Li, Z.; Liu, J.; McClain, J. D.; Sayfutyarova, E. R.; Sharma, S. et al. PySCF: the Python-based simulations of chemistry framework. *Wiley Interdiscip. Rev. Comput. Mol. Sci.* **2018**, *8*, e1340.

(37) Sun, Q.; Zhang, X.; Banerjee, S.; Bao, P.; Barbry, M.; Blunt, N. S.; Bogdanov, N. A.; Booth, G. H.; Chen, J.; Cui, Z.-H. et al. Recent developments in the PySCF program package. *Journal of Chemical Physics* **2020**, *153*, 024109.

(38) Sun, Q. Libcint: An efficient general integral library for Gaussian basis functions. *J. Chem. Theory Comput.* **2015**, *36*, 1664–1671.

(39) Neese, F. Software update: The ORCA program system—Version 5.0. *Wiley Interdiscip. Rev. Comput. Mol. Sci.* **2022**, *12*, e1606.

(40) Guo, Y.; Riplinger, C.; Becker, U.; Liakos, D. G.; Minenkov, Y.; Cavallo, L.; Neese, F. Communication: An improved linear scaling perturbative triples correction for the do-

main based local pair-natural orbital based singles and doubles coupled cluster method [DLPNO-CCSD (T)]. *J. Chem. Phys.* **2018**, *148*, 011101.

(41) Weber, J. L.; Churchill, E. M.; Jockusch, S.; Arthur, E. J.; Pun, A. B.; Zhang, S.; Friesner, R. A.; Campos, L. M.; Reichman, D. R.; Shee, J. In silico prediction of annihilators for triplet–triplet annihilation upconversion via auxiliary-field quantum Monte Carlo. *Chem. Sci.* **2021**, *12*, 1068–1079.

(42) Rudshteyn, B.; Coskun, D.; Weber, J. L.; Arthur, E. J.; Zhang, S.; Reichman, D. R.; Friesner, R. A.; Shee, J. Predicting ligand-dissociation energies of 3d coordination complexes with auxiliary-field quantum Monte Carlo. *J. Chem. Theory Comput.* **2020**, *16*, 3041–3054.

(43) Weber, J. L.; Vuong, H.; Friesner, R. A.; Reichman, D. R. The Design of New Practical Constraints in Auxiliary-Field Quantum Monte Carlo. 2023.

(44) Neese, F.; Valeev, E. F. Revisiting the Atomic Natural Orbital Approach for Basis Sets: Robust Systematic Basis Sets for Explicitly Correlated and Conventional Correlated *ab initio* Methods? *J. Chem. Theory Comput.* **2011**, *7*, 33–43.

(45) Nie, M.; Chalasani, D.; Abraham, D. P.; Chen, Y.; Bose, A.; Lucht, B. L. Lithium ion battery graphite solid electrolyte interphase revealed by microscopy and spectroscopy. *J. Phys. Chem. C* **2013**, *117*, 1257–1267.

(46) Shi, S.; Lu, P.; Liu, Z.; Qi, Y.; Hector Jr, L. G.; Li, H.; Harris, S. J. Direct calculation of Li-ion transport in the solid electrolyte interphase. *J. Am. Chem. Soc.* **2012**, *134*, 15476–15487.

(47) Leifer, N.; Smart, M.; Prakash, G.; Gonzalez, L.; Sanchez, L.; Smith, K.; Bhalla, P.; Grey, C.; Greenbaum, S. 13C solid state NMR suggests unusual breakdown products in SEI formation on lithium ion electrodes. *J. Electrochem. Soc.* **2011**, *158*, A471.

(48) Lee, T. J.; Taylor, P. R. A diagnostic for determining the quality of single-reference electron correlation methods. *Int. J. Quantum Chem.* **1989**, *36*, 199–207.

(49) Sandler, I.; Chen, J.; Taylor, M.; Sharma, S.; Ho, J. Accuracy of dlpno-ccsd (t): Effect of basis set and system size. *J. Phys. Chem. A* **2021**, *125*, 1553–1563.

(50) Demichelis, R.; Civalleri, B.; Ferrabone, M.; Dovesi, R. On the performance of eleven DFT functionals in the description of the vibrational properties of aluminosilicates. *Int. J. Quantum Chem.* **2010**, *110*, 406–415.